Experimental investigation on laminar burning velocities of ammonia/hydrogen/air mixtures at elevated temperatures

Charles Lhuillier, Pierre Brequigny, Nathalie Lamoureux, Francesco Contino, Christine Mounaïm-Rousselle

Experimental investigation on laminar burning velocities of ammonia/hydrogen/air mixtures at elevated temperatures

Charles LHUILLIER[a,b,c,1], Pierre BREQUIGNY[a], Nathalie LAMOUREUX[d] ,Francesco CONTINO[b,c], Christine MOUNAÏM-ROUSSELLE[a]

[a]*Univ. Orléans, INSA-CVL, EA 4229 - PRISME, F-45072, Orléans, France*

[b]*Vrije Univ. Brussel, FLOW - Thermo and Fluid Dynamics Research Group, Belgium*

[c]*Vrije Univ. Brussel, Univ. Libre Bruxelles, BURN - Combustion and Robust Optimization Joint Research Group, Belgium*

[d]*Univ. Lille, CNRS, UMR 8522 - PC2A - Physicochimie des Processus de Combustion et de l'Atmosphère, F-59000 Lille, France*

Abstract

The present study introduces new laminar burning velocity data for ammonia/hydrogen/air mixtures measured by means of the outwardly propagating spherical flame method at atmospheric pressure, for previously unseen unburned gas temperatures ranging from 298 to 473 K, hydrogen fractions ranging from 0 vol.% to 60 vol.% in the fuel and equivalence ratios in the range [0.8 – 1.4]. Results show increasing velocities with increasing hydrogen fraction and temperature, with maximum values obtained for rich mixtures near stoichiometry. The new experimental dataset is compared to dedicated laminar burning velocity correlations from the literature and to simulations using detailed kinetic mechanisms. The ammonia/air correlation presents a good agreement with measurements over the whole range of experimental conditions. The ammonia/hydrogen/air correlation captures the effect of the initial temperature satisfactorily for equivalence ratios below 1.3 and hydrogen fractions below 50 vol.% in the fuel, but discrepancies are observed in other conditions. The effect of hydrogen addition is reproduced satisfactorily for hydrogen fractions between 20 and 40 vol.% in the fuel, but discrepancies are observed for rich mixtures

[1] Corresponding author. Address: Laboratoire PRISME, Université d'Orléans, 8 rue Léonard de Vinci, 45072 Orléans, France. E-mail : charles.lhuillier@etu.univ-orleans.fr

Abbreviations. GD : Goldmann and Dinkelacker. LBV : Laminar Burning Velocity. OPSF: Outwardly propagating spherical flame. PDF: Probability density function. RES: Renewable Energy Sources. NTP: Normal Temperature and Pressure (298 K, 0.1 MPa)

below 20 vol.% hydrogen and for all mixtures containing 50 vol.% hydrogen and more. An optimization of both correlations is proposed thanks to the experimental data obtained, but only with partial improvement of the ammonia/hydrogen/air correlation. State-of-the-art detailed kinetic reaction mechanisms yield values in close agreement with the present experiments. They could thus be used along with additional experimental data from different techniques to develop more accurate correlations for time-effective laminar burning velocity estimates of NH_3/H_2/air mixtures.

Keywords

Ammonia, Hydrogen, Laminar Burning Velocity, Elevated temperature, Spherical vessel, Sustainable fuel

1. Introduction

In response to growing concerns regarding climate change, a majority of governments have agreed on common objectives to mitigate this phenomenon [1]. A recent report by the Intergovernmental Panel on Climate Change evaluated the possibilities and implications of a global warming limitation of 1.5°C above pre-industrial levels, that would alleviate the negative effects of climate change [2]. The report indicated that fossil-free Renewable Energy Sources (RES) should supply 52 to 67% of the total primary energy demand by 2050 in order to sufficiently cut carbon-based greenhouse gas emissions and thus ensure the warming limitation.

This transition will rely on diverse, mostly intermittent RES, such as wind or solar photovoltaic, and will thus require flexibility and grid-balancing strategies, as well as safe and efficient transport and storage. Power-to-Fuel strategies are promising options, in which excess electricity is used to produce hydrogen-based synthetic fuels in gaseous or liquid form. Those so-called electrofuels [3] present a high energy density (> 4-5 MJ/l), are stable in time (seasonal or long-term storage), can be transported over long distances and their production can be carbon-neutral. In spite of being already and increasingly recognized as a fuel, molecular hydrogen (H_2) presents major drawbacks caused by its high volatility and flammability, including the need for a tailored infrastructure and the associated storage and transport costs and safety issues.

Ammonia (NH_3) has received recent interest as a carbon-free electrofuel [4,5] with a relatively high energy density (13 MJ/l), as it can be stored in liquid form under 1.1 MPa at 300 K and its lower heating

value reaches 18.8 MJ/kg. Additionally, ammonia is already transported and stored safely at industrial scale, which makes it a promising complementary alternative to molecular hydrogen. Current annual production reaches 180 Mt worldwide, mostly from the Haber-Bosch process using steam methane reforming as the main H_2 source. However, renewable hydrogen from electrolysis could be used instead while ensuring a satisfactory stability of the Haber-Bosch process [6]. Grinberg Dana et al. showed that NH_3 exhibits the highest Power-to-Fuel-to-Power ratio when compared with methane, methanol and dimethyl-ether [7]. However, the high corrosiveness and toxicity of ammonia require thorough safety precautions, especially when final users are exposed.

Following these considerations, several studies focused on ammonia combustion, addressing many of the remaining challenges regarding NH_3 fundamental combustion properties, chemical kinetics modeling or combustion in gas turbines and internal combustion engines as single or dual fuel [8,9]. A major drawback of NH_3 as a fuel is its very low combustion intensity, as illustrated by its Laminar Burning Velocity (LBV), which is one order of magnitude smaller than that of conventional hydrocarbons in atmospheric conditions [10–17]. This represents a challenge for NH_3 as a fuel in practical combustion systems, but also for laminar flame experiments themselves, as noted by Pfahl et al. [12], Takizawa et al. [14] and Hayakawa et al. [15]. Indeed, as a function of the mixture composition, ignition energies have to be significantly higher than in the case of conventional hydrocarbons. Moreover, as the LBV for NH_3/air mixtures is very slow, the buoyancy effect can cause an outwardly propagating spherical flame (OPSF) to propagate upward as well as outward, thus losing its spherical shape and compromising the measurement.

Several experimental studies have considered enhancing the combustion by seeding NH_3 with H_2, which could conveniently be obtained from ammonia decomposition, leading to a significant increase in the LBV and extending the flammability ranges. Lee et al. investigated the combustion properties of NH_3/H_2/air premixed laminar OPSFs as a function of hydrogen fractions in the fuel blend, for several equivalence ratios from fuel-lean to fuel-rich at Normal Temperature and Pressure (NTP), i.e. 298K, 0.1 MPa [18,19]. Li et al., by using the Bunsen burner method, provided LBV measurements for various NH_3/H_2/air mixtures at NTP as a function of equivalence ratios [20]. Ichikawa et al. investigated the LBV and Markstein length of several NH_3/H_2/air stoichiometric mixtures by means of the OPSF method also at 298 K but for an initial

pressure ranging from 0.1 to 0.5 MPa [21]. Han et al. reported LBV measurements obtained by means of the heat flux method, with NH_3 blended with H_2, CO or CH_4 as fuels and air as the oxidizer at NTP [22]. Kumar and Meyer conducted Bunsen burner experiments for different NH_3/H_2 blends at NTP, but their results contradict those of the previously mentioned studies [23].

All these studies reported that the addition of hydrogen to an NH_3 blend significantly increased the LBV with a maximum value around an equivalence ratio of 1.1. However, only partial agreement is found between the different literature sources and the LBV dataset for NH_3/H_2/air flames remains significantly limited, especially at temperatures above 300 K and pressures above 0.1 MPa. Moreover, the comparisons between LBV measurements and numerical simulation results found in the literature show a remaining potential for the improvement of the chemical kinetic mechanisms. For instance, Ichikawa et al. [21] showed only qualitative agreement between their experimental LBVs and those obtained with the mechanisms of Miller et al. [24], Lindstedt et al. [25], Tian et al. [26] and Konnov [27], just as Han et al. [22] exhibited discrepancies between their experiments and the mechanisms of Okafor et al. [28] among others. Recently, Cavaliere et al. [29] conducted a survey on ten chemical kinetic mechanisms including NH_3/H_2 chemistry and selected those of Okafor et al. [28], Mathieu and Petersen [30] and Otomo et al. [31] to be reduced, so as to decrease their computational cost. However, they still report a significant scatter in the results obtained by the different mechanisms and see potential for further improvement in the NH_3 and NH_3/H_2 sub-mechanisms.

As the use of chemical kinetic mechanisms in simulations remains very computationally intensive, Goldmann and Dinkelacker proposed semi-empirical correlations, called GD correlations in the following, for the LBV of NH_3/air, NH_3/H_2/air and $NH_3/H_2/N_2$/air mixtures [32]. These semi-empirical correlations were based on the correlation by Metghalchi and Keck [33], by considering the LBV dataset available and estimates obtained thanks to the detailed ammonia oxidation mechanism of Mathieu and Petersen [30]. The correlations are simple, making them very useful to be included in computationally intensive CFD simulations. The LBV is given as a function of the global equivalence ratio, the hydrogen amount, the nitrogen ratio (to simulate dilution) and the unburned temperature and pressure, following the form in Eq. 1:

$$s_{\mathrm{u}}^{0} = s_{\mathrm{u,ref}}^{0} T_{\mathrm{n}}^{\alpha} p_{\mathrm{n}}^{\beta} \gamma \kappa, \#(1)$$

[Tapez ici]

where $s_{u,ref}^{0}$ is a reference velocity depending only on the fuel mixture composition and the equivalence ratio, T_n and P_n the normalized unburned gas temperature and pressure respectively, γ a factor to model the effect of nitrogen dilution (when relevant) and κ a correction factor to fit the correlations to the experimental values from the literature. Since literature data included only measurements around 300 K and pressure up to 0.5 MPa, the κ factor was determined by considering only these conditions in the GD correlations. The proposed correlations were found to agree very well with the experimental data available in the literature, as well as with results from kinetics simulations using the detailed reaction mechanism of Mathieu and Petersen from which they were derived. Since those simulation results showed no abrupt behavior and an improved accuracy when increasing the pressure, Goldmann and Dinkelacker concluded that the mechanism could be extrapolated to pressures above its validation range, and therefore made the same assumption for their correlations.

However, this conclusion remains uncertain, as is the accuracy of the reaction mechanisms and LBV correlations for NH_3/air and NH_3/H_2/air mixtures at elevated temperature (above 300 K), due to the lack of experimental literature data under such conditions for validation purposes. The objective of the present study was to partially fill this lack of data by introducing new LBV measurements of NH_3/air and NH_3/H_2/air outwardly propagating spherical flames at 0.1 MPa of pressure for unburned gas temperatures up to 473 K. The GD correlations are also discussed with respect to the new experimental data and an optimization attempt is presented.

2. Experimental and numerical methods

2.1. Experimental set-up

We carried out the experiments in a 4.2 dm^3 stainless steel spherical vessel that can be heated up to 473 K by an incorporated resistive coil. A type-K thermocouple and a piezoelectric pressure transducer were used to monitor the temperature T_u and pressure P_u inside the chamber, respectively. The filling procedure was already described in a previous study on a similar set-up [34] and is thus only briefly summarized here. A vacuum pump is used to empty the vessel to a residual pressure of less than 1 kPa and the preheated reactive gases are then introduced thanks to Brooks 5850S thermal mass flowmeters, while being stirred by a fan to ensure a homogeneous mixture. Bottled gases are used, including synthetic air with 20.9% ± 0.2% oxygen

and a 99.999% purity, hydrogen with a 99.999% purity and ammonia with a 99.98% purity. After the intake, a quiescent phase of 10 s is set in order to avoid any undesired fluid motion. Then, a discharge energy is delivered for ignition at the center of the chamber thanks to two 1 mm tungsten electrodes. The spark gap can be adjusted from 1 to 3 mm to favour ignition under lean conditions with a high ammonia content.

2.2. Experimental conditions

The global stoichiometric combustion reaction of NH_3/H_2/air is:

$$\left(1 - x_{H_2}\right)NH_3 + x_{H_2}H_2 + \frac{3 - x_{H_2}}{4}(O_2 + 3.76N_2) \rightarrow \left(\frac{3 - x_{H_2}}{2}\right)H_2O + \left(\frac{13.28 - 5.76x_{H_2}}{4}\right)N_2 \quad \#(2),$$

with x_{H_2}, the hydrogen molar fraction in the fuel mixture. The global equivalence ratio ϕ is defined as:

$$\phi = \frac{\frac{X_{H_2} + X_{NH_3}}{X_{air}}}{\left(\frac{X_{H_2} + X_{NH_3}}{X_{air}}\right)_{st}}, \#(3)$$

where X_s represents the molar fraction of the species *s* in the reactive mixture. The experimental conditions are summarized in Table 1. In some boundary cases, such as fuel-lean (resp. fuel-rich) mixtures with $\phi \leq 0.9$ (resp. $\phi \geq 1.2$) and a small hydrogen fraction, the mixture ignition fails to induce flame propagation or buoyancy instability phenomena alter the flame propagation too much to extract meaningful data and such cases are thus left aside.

Table 1. Experimental conditions

P_u (MPa)	T_u (K)	x_{H_2}	ϕ
0.1	{298 ; 323 ; 373 ; 423 ; 473}	[0 – 0.6]	[0.8 – 1.4]

2.3. Image processing

In the cases with sucessful laminar flame propagation, double Schlieren images of the flame are recorded from two orthogonal angles through two pairs of opposite quartz windows (70 mm diameter) by a Phantom v1210 high-speed CMOS camera, as fully described in [35]. The frame acquisition rate of the camera is adjusted with respect to the propagation velocity of the flame up to 18000 fps, in order to maximize the

number of usable images. Following recommendations by Huo et al. [36], a minimum number of 30 images is considered for post-processing. The double Schlieren configuration allows the detection of flame instabilities, but only one view is used to extract the LBV. An example of a flame image is shown in Figure 1.

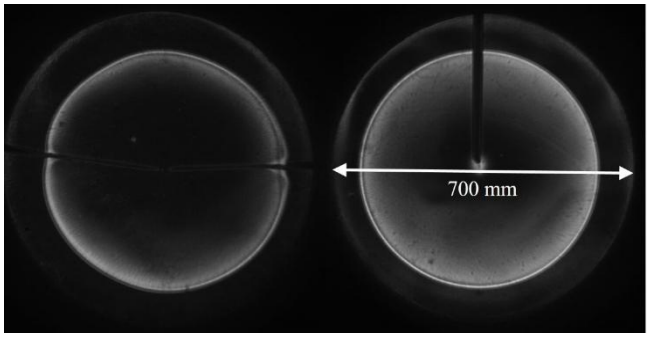

Figure 1. Double Schlieren view at time t of a stable NH_3/H_2/air flame at 0.1 MPa and 473 K.

The radii of the spherical flames are extracted using an image postprocessing algorithm with background substraction. The range of the flame radius R_f used for the analysis is manually kept between roughly 6.5 and 25 mm in order to eliminate the spark ignition and wall-pressure confinement effects. The pressure measured in the vessel remains constant over the whole analysis range. The stretched laminar flame propagation velocity s_b is calculated as a first-order gradient $s_b = dR_f/dt$, since the burned gas is assumed to be quiescent. Assuming that the flame is adiabatic and the propagation quasi-steady, s_b is then extrapolated to zero stretch using the nonlinear Equation 4 proposed by Kelley and Law [37], based on an asymptotic analysis by Ronney and Sivashinsky [38] and validated by Halter et al. for methane and isooctane/air flames [39]:

$$\left(\frac{s_b}{s_b^0}\right)^2 \ln\left(\frac{s_b}{s_b^0}\right)^2 = -\frac{2L_b K}{s_b^0}. \#(4)$$

The flame stretch K is calculated according to $K = 2/R_f * dR_f/dt$ for a spherical flame, L_b is the Markstein length and s_b^0 the unstretched flame propagation velocity of the burned state, respectively.

The laminar burning velocity is finally calculated from the continuity equation through the flame surface, $s_u^0 = \rho_b/\rho_u * s_b^0$, where burned and unburned gas densities are calculated from equilibrium calculations.

2.4. Uncertainty considerations

[Tapez ici]

The validation of kinetic mechanisms requires accurate measurement data including quantitative uncertainty ranges. In the present study, a method based on the work of Moffat [40] and developed by Brequigny et al. [41] was implemented for uncertainty quantification.

The experimental errors are of two kind and described as experimental hardware errors $(\Delta s_u^0)_{P,T,X_s}$, reflecting the accuracy of the initial temperature, pressure and mixture composition monitoring, and imaging errors $(\Delta s_u^0)_{\text{imaging}}$, both from the imaging technique itself and the processing.

The temperature and pressure error terms are determined by using the correlations by Goldmann and Dinkelacker [32] in Eq. 1, as $|\alpha| \cdot \Delta T/T$ and $|\beta| \cdot \Delta P/P$ respectively. The exponents α and β, which are functions ϕ and x_{H_2} are calculated for each test condition. In most cases, the combined error from those two terms is significantly smaller than ± 2%, but can be higher in a few cases at 298 K initial temperature, due to the difficulty of maintaining the vessel temperature after several combustion tests, without exceeding ± 8%.

The uncertainties on the mixture composition are due to the accuracy of the mass flow meters (1% of the full scale) and propagate on the LBV through ϕ and x_{H_2}. Depending on the representation of s_u^0 chosen in this article, either ϕ or x_{H_2} can be a variable, while the other is a fixed parameter. While the uncertainty on the variable must be indicated with horizontal error bars, that on the fixed parameter(s) must be propagated in the depicted LBV. Since the LBV dependence on those parameters in the GD correlations is complex, the propagation of the uncertainty could hardly be formulated analytically as for the temperature and pressure errors. It was thus estimated by means of a Monte Carlo method as follows. The set point value of the fixed parameter (ϕ or x_{H_2}) is considered as the mean value of a normal probability density function (PDF), whose standard deviation is given by the uncertainty on the parameter. During a great number of N = 10 000 iterations, a random value is taken for the parameter following that PDF. The LBV is then calculated by means of the corresponding GD correlation for each iteration, all other parameters and variables remaining unchanged. For each initial condition, a normal PDF for the LBV is obtained this way, of which the standard deviation is considered to be the propagated uncertainty of ϕ or x_{H_2} on the LBV. The empirical correction factor κ of the GD correlations (Eq. 1) was applied only when $x_{H_2} < 0.5$, as it degrades strongly the prediction capability of the ϕ and x_{H_2} dependences at higher hydrogen fuel fractions, as will be seen in

Section 3. Overall, the LBV uncertainty resulting from mixture composition errors is thought to be conservative.

Another uncertainty source associated with the OPSF technique is radiation-induced uncertainty. Yu et al. showed that radiative losses affect the LBV of OPSFs by reducing the flame temperature and by inducing an inward flow in the burned gas due to radiation cooling [42]. They proposed a fuel independent correlation for the determination of the radiation-induced relative error on the LBV in such flames, which is a decreasing function of the LBV and depends on T_u linearly. However, that correlation was only validated numerically in the case of different hydrocarbon fuels and syngas, and it is unclear whether it is applicable in our case, especially due to the absence of CO_2 in the burned gas of NH_3/H_2/air flames. A recent numerical study by Nakamura and Shindo [43] showed a significant impact of radiative heat losses on the LBV of NH_3/air flames using simulations of 1D freely propagating premixed flames with their own reaction mechanism [44]. Under NTP conditions, the relative error increased away from stoichiometry and reached about 13 % for ϕ = 0.8, 3 % for ϕ = 1.0 and about 8 % for ϕ = 1.4, corresponding to absolute errors of a few millimeters per second. However, those results do not take into account the spherical geometry of the presently studied flames and depend on the accuracy of the reaction mechanism that was used. Those considerations are summarized in Figure 2 for NH_3/air flames at NTP, which are the most radiation-affected conditions due to very low LBVs. The simulation results of Nakamura and Shindo are plotted together with similar simulations that we carried out in ChemkinPro [45] (see Sec. 2.5) with the absorption coefficients in [43] and the detailed reaction mechanism of Otomo et al. [31], as well as results obtained by applying the correlation of Yu et al. to present experimental data. Figure 2 highlights the dependence of the radiation-induced error on the LBV, and shows good agreement between the different estimates. Therefore, the correlation of Yu et al. was used presently as the best estimate for the radiation-induced uncertainty, $(\Delta s_u^0)_{\text{radiation}}$, added only in the positive uncertainty $+ U_{s_u^0}^{95\%}$, and decreasing with increasing LBV down to less than 1% for fast flames. The same estimation method was recently used by Mei et al. [17].

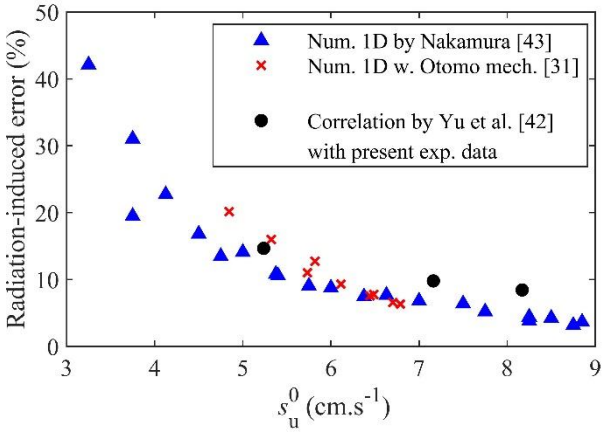

Figure 2. Relative radiation-induced uncertainty on the LBV of NH_3/air flames at NTP.

The repeatability of the tests is assessed by conducting a minimum number n of three measurements for each initial condition. The standard deviation proves the repeatability of the measurements and is used to calculate the statistical error in the form of a 95% confidence interval by means of a Student's t-distribution, as in Eq. 5:

$$\left(\frac{\Delta s_u^0}{s_u^0}\right)_{\text{statistical}} = t\frac{\sigma_{s_u^0}}{\sqrt{n}} \#(5)$$

with t, the value of the Student's density function (t = 3.182 for n = 3). The statistical error exceeds 10% in a small number of cases, generally under very lean or rich conditions, where the flame propagation is mostly affected by perturbations. In general, this value is below 5% and down to 0.1%.

The experimental error terms are finally combined with the imaging error, the radiation error and the statistical error obtained by repeating several identical measurements to calculate the overall uncertainty, $U_{s_u^0}^{95\%}$, given in Eq. 6:

$$U_{s_u^0}^{95\%} = \sqrt{(\Delta s_u^0)_T^2 + (\Delta s_u^0)_P^2 + (\Delta s_u^0)_{X_s}^2 + (\Delta s_u^0)_{\text{imaging}}^2 + (\Delta s_u^0)_{\text{radiation}}^2 + (\Delta s_u^0)_{\text{statistical}}^2} \#(6)$$

Therefore, all the data are presented in the following figures with the average LBV values along with the overall uncertainty, $\overline{s_u^0} \pm U_{s_u^0}^{95\%}$, meaning that the error bars can be assimilated to 95% confidence intervals. All the uncertainties are reported in the Supplementary Material.

2.5. Numerical modelling

[Tapez ici]

LBV simulations were performed with Ansys ChemkinPro [45] by using three detailed kinetic mechanisms for NH_3/H_2/air combustion [30,31,44]. Otomo's model [31] was validated against experimental results including LBVs obtained in various NH_3/H_2/Air mixture at ambient temperature and 0.1 MPa. Nakamura's model [44] was validated against NH_3/air weak flames in micro flow reactor, including species profiles measurements. Both mechanisms reveal the importance of intermediate species such as NH_2, HNO and N_2Hx. The third one by Mathieu and Petersen [30] was mostly validated against ignition delay times and was selected by Goldman and Dinkelacker [32] to fit their semi-empirical correlations.

The intercomparison between the experimental values and results from full kinetic computations was limited to 2 cases, but in the entire range of equivalence ratio [0.8-1.4]. First, the unburned temperature is set to 473K, and x_{H_2} is varied between 0 and 0.6. Second, the temperature varies in the entire range of the experiments, but x_{H_2} is fixed equal to 0.6. Those are the conditions of maximal discrepancy between the GD correlations and the present experiments, as it will be seen in Sec. 3.

3. Results and discussion

This section presents the main experimental results and compares them to the LBV values estimated by means of the detailed kinetic mechanisms in Sec. 2.5 and the GD correlation. The experimental corrective factor κ defined in Section 1 is always applied in the GD correlations with the values given in [30], unless otherwise stated. The extensive dataset obtained during the present study is available in the Supplementary Material.

3.1. Effect of the equivalence ratio

Figure 3 shows a comparison of the present LBV measurements with experimental literature data and the GD correlation for NH_3/air flames under NTP. The very low LBVs result in a significant scatter in the experimental data, due to technique-dependent uncertainties that are exacerbated by the instability phenomena already described in Sec. 1 and Sec. 2.2 for the OPSF technique. While the data for stoichiometric flames show a good general consistency across the studies, lean and rich flames exhibit differences between the measurements up to more than 2 cm/s. While this discrepancy might seem reasonable in other cases, it represents presently an error of more than 50%, due to the very low LBVs. Present measurements are in the middle of the literature scatter, including very recent measurements with

different techniques by Han et al. [22] and Mei et al. [17]. Error bars are asymmetric due to the positive-only radiation-induced uncertainty, which is especially significant at low LBVs.

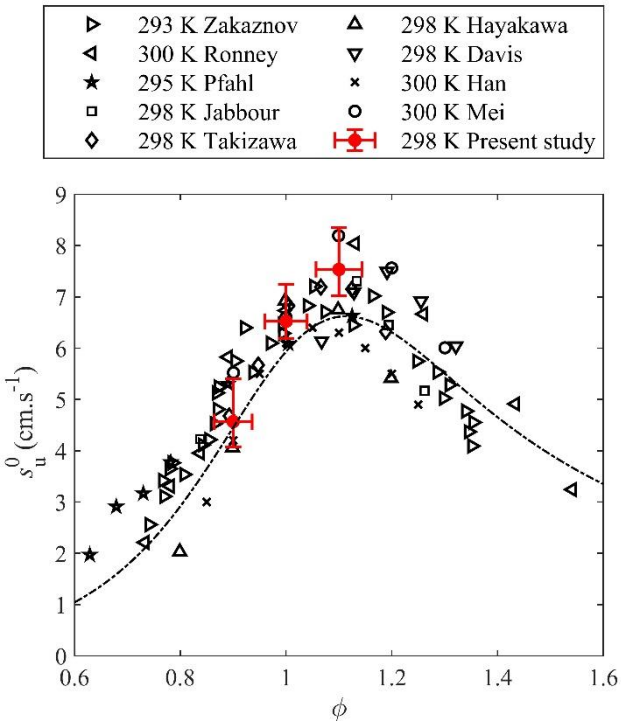

Figure 3. Laminar burning velocities of NH_3/air flames under atmospheric conditions. Symbols: experiments. Line: GD correlation at 0.1 MPa, 298 K [32].

Figure 4 shows the variation of the measured LBV as a function of the equivalence ratio over the whole temperature range for NH_3/air and NH_3/H_2/air flames, along with experimental data from the literature close to 298 K and 0.1 MPa and GD correlations values. For NH_3/H_2/air flames, present measurements at 298 K are in reasonable agreement with the experimental literature data. For $x_{H_2} = 0.05$ (Fig. 4b), good agreement is found with Ichikawa et al. [21] at stoichiometry, while a small discrepancy is observed with Han et al. [22]. For $x_{H_2} = 0.3$ (Fig. 4c), the present measurements partially agree with those of Lee et al. [19] and a very good agreement is found with Han et al. at stoichiometry. For $x_{H_2} = 0.4$ (Fig. 4d), our values agree with those of Han et al. for equivalence ratios between 0.8 and 1.2, and disagree for ϕ = 1.3 and 1.4, while a slight mismatch is observed with a value of Ichikawa et al. at stoichiometry. For $x_{H_2} = 0.5$ (Fig. 4e), very good agreement is found with the data of Li et al. [20], except for ϕ = 1.4 and partial agreement is observed

[Tapez ici]

with the data of Lee and coworkers. For $x_{H_2} = 0.6$ (Fig. 4f), present values agree with those of Li et al. only below stoichiometry, and a good agreement is found at stoichiometry with Ichikawa and coworkers. Overall, a comparative assessment of the uncertainties relative to LBV measurement using different methods would be of interest in the case of NH_3/H_2/air flames, along with additional measurements with various techniques, in order to evaluate the reliability of the global dataset. This is however beyond the scope of the present work.

The measured LBVs present a classical bell shape as a function of the equivalence ratio, with a maximum near ϕ = 1.1 for all temperatures and hydrogen fractions up to $x_{H_2} = 0.5$. However, for mixtures with $x_{H_2} = 0.6$, the variation in the experimental LBV as ϕ varies becomes smaller around the maximum due to the effect of hydrogen, resulting in a relatively "flatter" shape of the data distribution and a slight shift of the maximum towards ϕ = 1.2, as illustrated in Fig. 4f. At T_u = 373 K for instance, this results in a relative increase of about 30 % of the LBV between ϕ = 0.9 and ϕ = 1.1, and a decrease of 18% between ϕ = 1.1 and ϕ = 1.3 for $x_{H_2} = 0.3$, while the relative increase and decrease reach only 13 % and 5 % respectively for $x_{H_2} = 0.6$.

The NH_3/air GD correlation reproduces well the shape of the LBV as a function of ϕ, even at elevated temperatures, as shown in Fig. 4a. The shape is also relatively well reproduced by the NH_3/H_2/air GD correlation for $0.2 \leq x_{H_2} \leq 0.4$, as illustrated in Fig. 4c and 4d for x_{H_2}= 0.3 and 0.4. Those are cases where the effect of the equivalence ratio in the GD correlation was validated against literature measurements at NTP conditions. In the cases for which limited experimental data were available or only data that do not agree with the present results, the NH_3/H_2/air GD correlation fails to reproduce accurately the shape of the present measurements. In particular for $x_{H_2} = 0.05$, Fig. 4b shows that the correlation underestimates the LBVs for rich mixtures at all temperatures. The correlation values are not symmetric with respect to the maximum LBV, which is underestimated itself both in its magnitude and equivalence ratio of occurrence as compared to the experiments. Fig. 4f shows that when $x_{H_2} = 0.6$ the estimated shape is symmetric, but does not accurately reproduce the much "flatter" shape of the present experimental points, especially at higher

[Tapez ici]

temperatures. Thus, the availability of reliable experimental LBV data seems to be critical for the behavior of the GD correlations with respect to the equivalence ratio, when the original correction factor κ is applied.

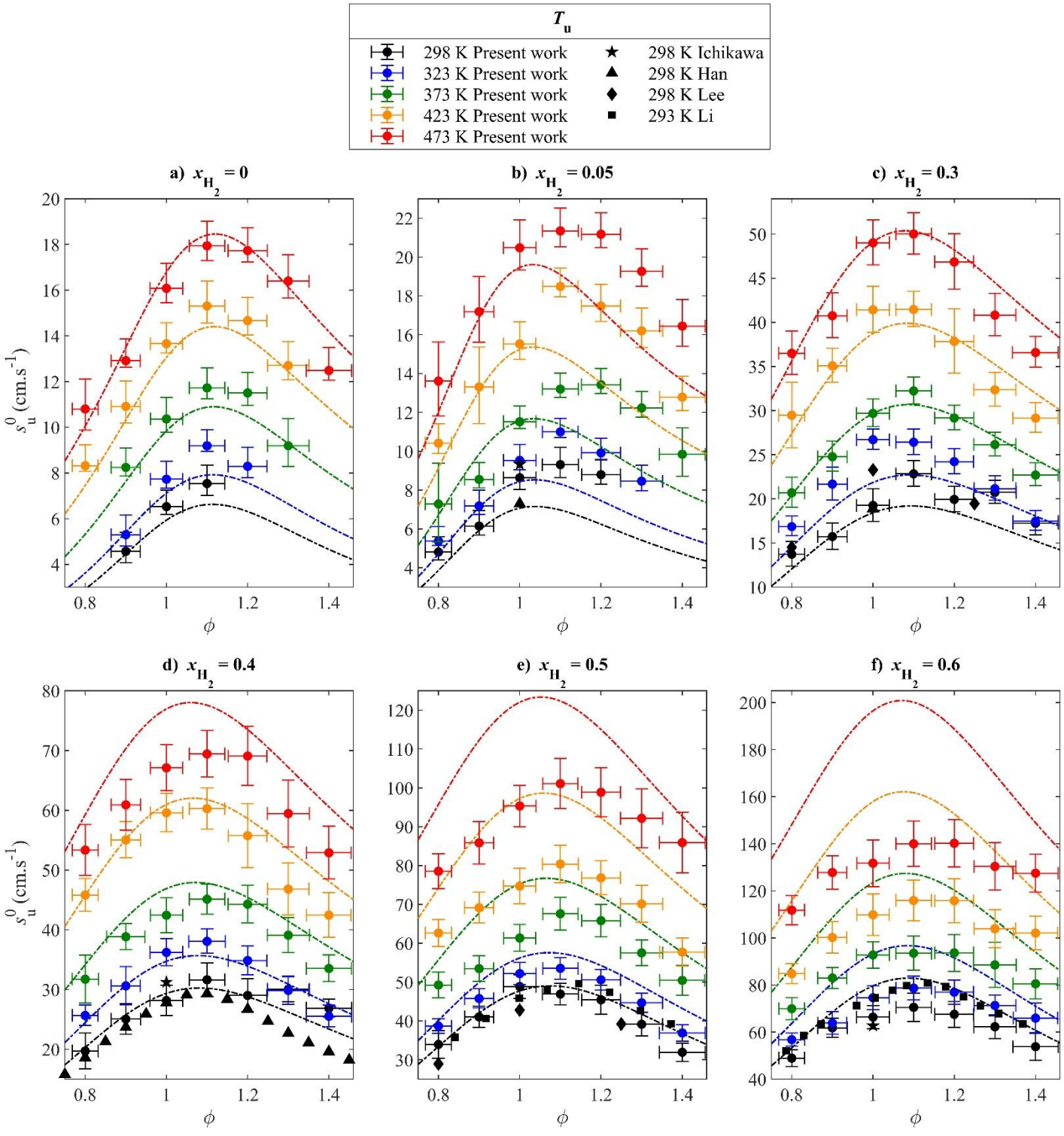

Figure 4. Laminar burning velocities of NH_3/air and NH_3/H_2/air mixtures at P_u = 0.1 MPa. Symbols: experiments; vertical error bars are 95% confidence intervals. Lines: GD correlation [32].

3.2. Effects of hydrogen enrichment

[Tapez ici]

The influence of the fuel hydrogen fraction on the LBV is presented in Fig. 5 at NTP conditions. For the sake of readability, only three equivalence ratios are depicted, along with corresponding LBV data from the literature and GD correlation values. Note that the Bunsen burner study of Li et al. [20] did not always provide data at the exact equivalence ratios that are depicted, so the closest values were plotted. The LBV exhibits an exponential increasing trend with volumetric hydrogen addition in the fuel. Present LBV measurements agree well with available literature data for a large majority of cases, as well as with GD correlation values. However, significant discrepancies are noticed for $x_{H_2} > 0.5$ and $\phi \geq 1.0$, as noted in Sec. 3.1. In those conditions, the present data agree with the value of Ichikawa et al. [21], but disagree with the data of Li et al. [20] and the correlation. The good agreement between the correlation and Li et al.'s data is explainable by the high relative weight of that experimental dataset in the NH_3/H_2/air LBV literature at the time of establishing the correlation. The latter was thus mainly fitted on that dataset, through the correction factor κ. Therefore, the accuracy of the measurements at high hydrogen fractions in the fuel might be questioned, with respect to the chosen experimental method. The OPSF method used by Ichikawa et al. and the present authors yields closely agreeing values at ϕ = 1.0. Under NTP conditions, the GD correlation slightly underestimates present LBVs when $\phi \geq 1.0$ and $0.05 \leq x_{H_2} \leq 0.2$, agrees well with all measurements for $0.2 < x_{H_2} \leq 0.5$, and significantly overestimates LBVs for $x_{H_2} > 0.5$ and $\phi \geq 1.0$. The data of Lee et al. [19] show slight discrepancies with the other data and the correlation but remain in the trend. However, the data of Kumar et al. [23] are off the trend and will thus be left aside in the considerations of Sec. 3.4, as it was originally the case when the GD correlation was developed in [32].

[Tapez ici]

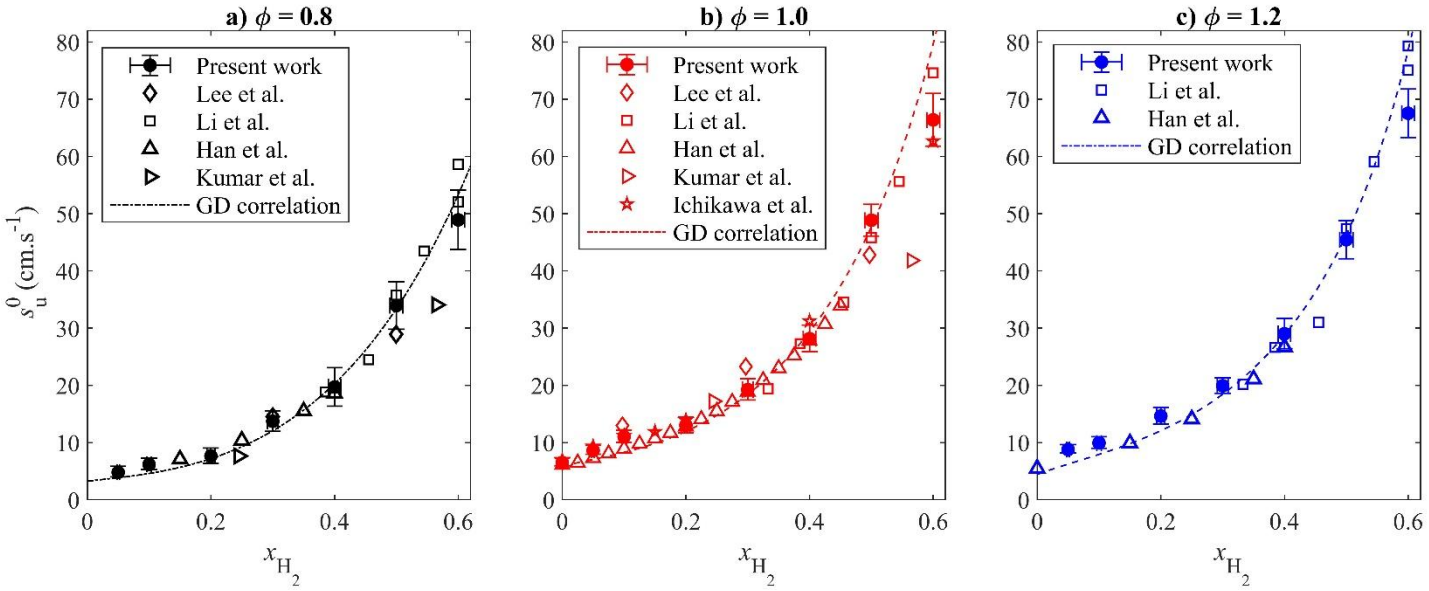

Figure 5. Laminar burning velocities of NH_3/H_2/air mixtures at T_u = 298 K and P_u = 0.1 MPa. Symbols: experiments; vertical error bars are 95% confidence intervals. Lines: GD correlation [32].

The behavior of the GD correlation with respect to the hydrogen fraction is confirmed by LBV measurements at higher temperatures, as shown in Figure 6 in the case $\phi = 1.1$, where the maximum LBV value is reached in most conditions. The measured and estimated values both exhibit exponential increasing trends as a function of the fuel hydrogen fraction for all temperatures, but with different slopes when depicted in a logarithmic scale. A general underestimate of the present data by the GD correlation is observed for low hydrogen fractions, while the LBVs at high hydrogen fractions are largely overestimated. However, the correlation is in close agreement with data of Han et al. [22] up to 40% H_2 at T_u = 298 K.

It should be noted that only the correlation for NH_3/H_2/air mixtures was plotted here. The NH_3/air correlation agrees much better with experimental values for $x_{H_2} = 0$, as previously seen in Fig. 4a. So, a lack of continuity is observed between the NH_3/H_2/air and NH_3/air correlations when the hydrogen fraction becomes very small. Again, this is likely a consequence of the limited availability of accurate measurement data for correlation fitting at the time it was established. Since most of the previously available data were within the range $0.3 \leq x_{H_2} \leq 0.6$, the best correlation prediction is found here. It should be noted here that the mechanism by Mathieu and Petersen [30], used also to establish the correlation, is found to underestimate, respectively overestimate, the LBV of mixtures with low, respectively high hydrogen content [32].

[Tapez ici]

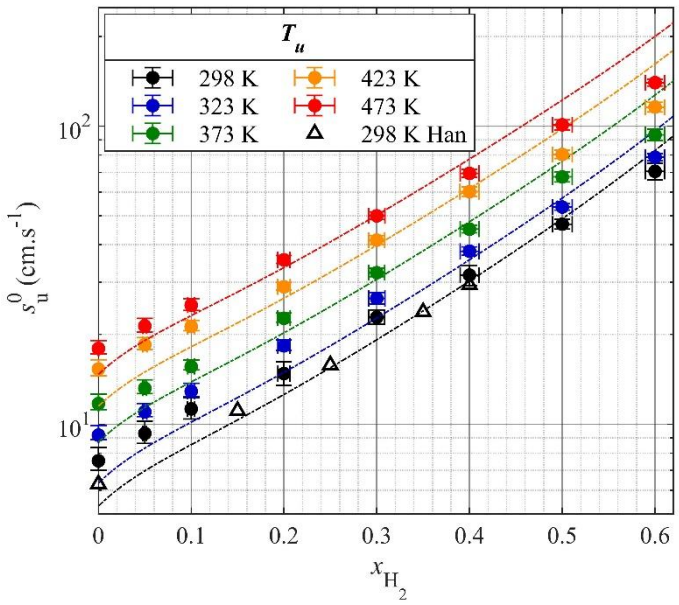

Figure 6. Laminar burning velocities of NH_3/H_2/air mixtures at P_u = 0.1 MPa and ϕ = 1.1. Filled symbols: present measurements. Hollow triangles: measurements of Han et al. [22]. Lines: GD correlation [32].

This is partly confirmed by Figure 7 that shows the evolution of the LBV with x_{H_2} at 473 K. Present measurements are compared with GD correlation values and simulations results using the detailed kinetic mechanisms introduced in Sec. 2.5. In such conditions, the mechanism of Mathieu and Petersen underestimates the experimental LBVs when ϕ = 0.8, when ϕ = 1.0 and $x_{H_2} < 0.5$ and when ϕ = 1.2 and $x_{H_2} < 0.5$. The mechanism of Otomo et al. is found to slightly underestimate the LBV in most cases, especially for intermediate hydrogen fuel fractions. The mechanism of Nakamura et al. shows the best overall agreement with the present data at elevated temperature as a function of the hydrogen fuel fraction. The GD correlation estimates diverge significantly from both the experimental and kinetic modelling trends when x_{H_2} increases, even though it is based on the Mathieu and Petersen mechanism. This is probably a consequence of the scarcity and accuracy of the available experimental dataset at high hydrogen fractions used to fit the correlation in the first place, through the correction factor κ that is applied here. The behavior of the correlation without applying κ is much closer to the Mathieu and Petersen's mechanism (no plotted here for readability), and yields thus accurate estimates for $x_{H_2} \geq 0.5$.

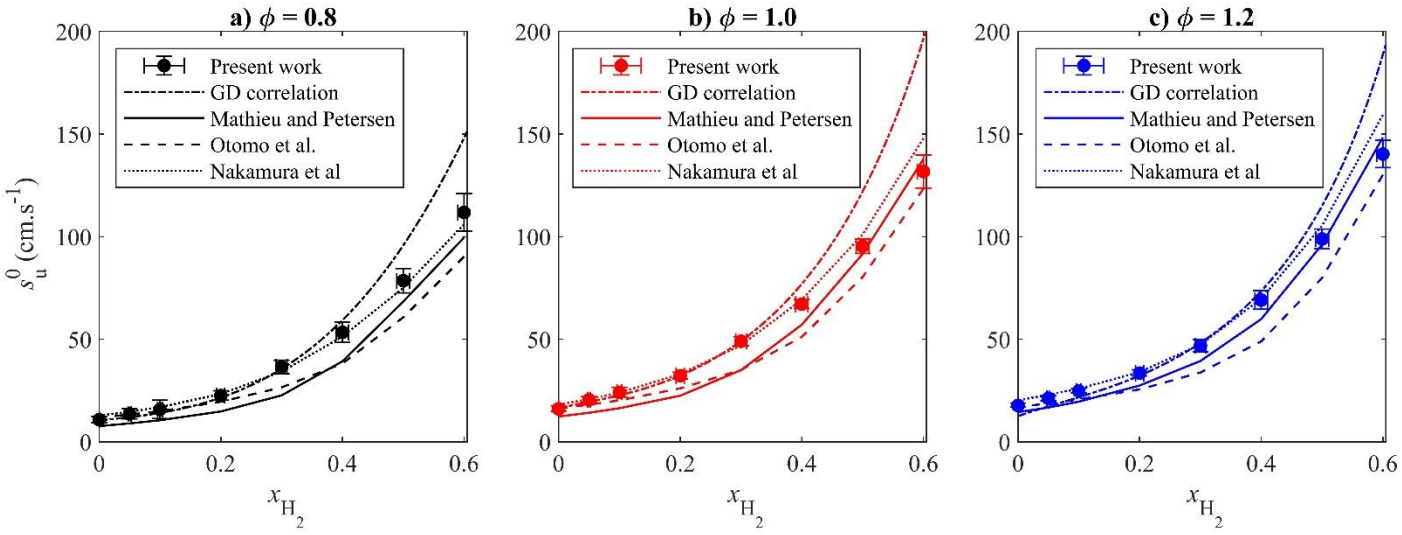

Figure 7. Laminar burning velocities of NH_3/H_2/air mixtures at P_u = 0.1 MPa and T_u = 473 K. Symbols: experiments. Lines: numerical models.

3.3. Effects of the temperature increase

Increasing the unburned gas temperature leads to an increase in the LBV and allows a more stable flame propagation in most cases. The respective influences of the equivalence ratio and hydrogen fraction on the LBV remain qualitatively unchanged when the temperature is increased: the experimental data distributions keep similar bell shapes in Fig. 4 and the slopes of the different distributions remain approximately parallel in Fig. 6 with increasing temperature.

The influence of the unburned gas temperature on the LBV is well estimated by the NH_3/air GD correlation (Fig. 4a), as well as by the NH_3/H_2/air GD correlation when $x_{H_2} = 0.05$ for lean mixtures (Fig. 4b) and when $0.2 \leq x_{H_2} \leq 0.4$ (Figs. 4c and 4d). In order to isolate the temperature effect, the values of the temperature exponent, α, assuming an exponential temperature dependence of the LBV as in Eq. 1 are depicted in Figure 8 as a function of the H_2 fraction. The experimental values of α, as well as the associated uncertainties were estimated by means of a Monte Carlo method to allow for the propagation of the uncertainties on the LBV measurements as described in Sec. 2.4. For each test point and each iteration, α is determined as the slope of $\ln(s_u^0) = f(\ln(T_u))$ by means of a least-squares linear regression, where s_u^0 is randomly chosen from a normal PDF with the average measured LBV as mean value and the global positive LBV uncertainty as standard deviation. The mean value and standard deviation of the resulting α-

distribution are taken as the best guess and uncertainty for α. Results show satisfactory agreement with the values given by the GD correlations, as a function of both the equivalence ratio and the hydrogen fraction, indicating the ability of the correlation to accurately estimate the temperature effect in most cases. However, no agreement is found between the experimental and estimated temperature behavior when the fuel contains 50% H_2 or more.

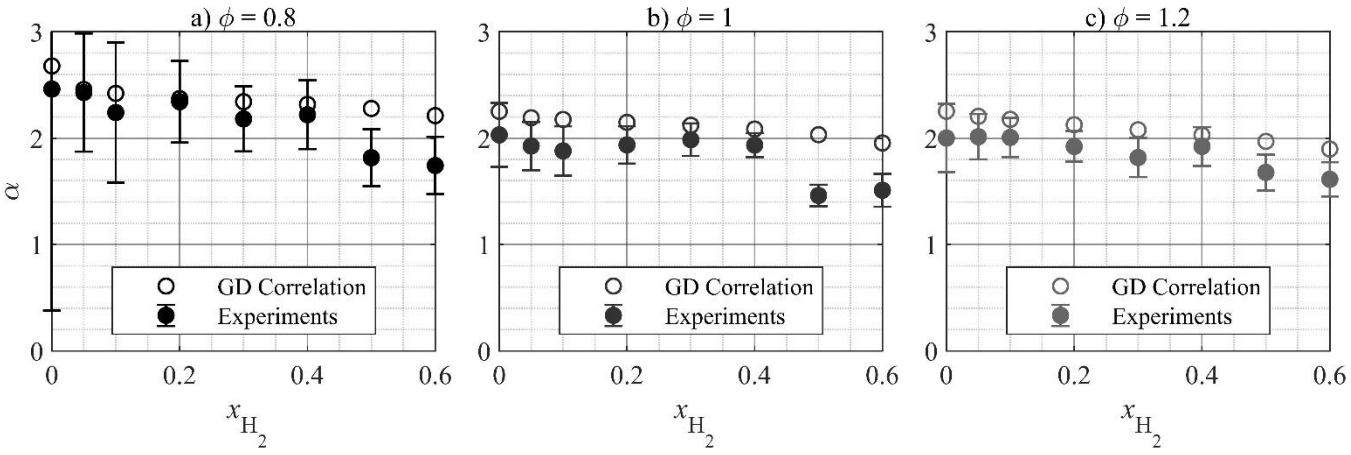

Figure 8. Temperature dependence of the LBV. α: temperature exponent as in Eq. 1.

This is emphasized in Figure 9, where the experimental LBVs are shown as a function of the initial gas temperature along with the GD correlation and results from kinetic simulations for x_{H_2} = 0.6. Again, the estimations by the GD correlation diverge away from the experimental trend and the kinetic model estimations, in particular those obtained with Mathieu and Petersen's mechanism for the same reasons mentioned in Sec. 3.2. While the different kinetic reaction mechanisms tested here show similar trends with respect to the temperature effect on the LBV, their estimations remain scattered and do not completely agree with the present measurements. While the mechanism of Otomo et al. generally underestimates the LBVs (as emphasized in the Supplementary Material), the mechanisms of Mathieu and Petersen agrees well, while the one of Nakamura et al. slightly overestimates the experimental data for rich mixtures. It should be remembered here that the error bars shown in Fig. 9 are considered to be conservative due to the use of the GD correlation to estimate the uncertainty caused by the mixture composition error as explained in Sec. 2.4.

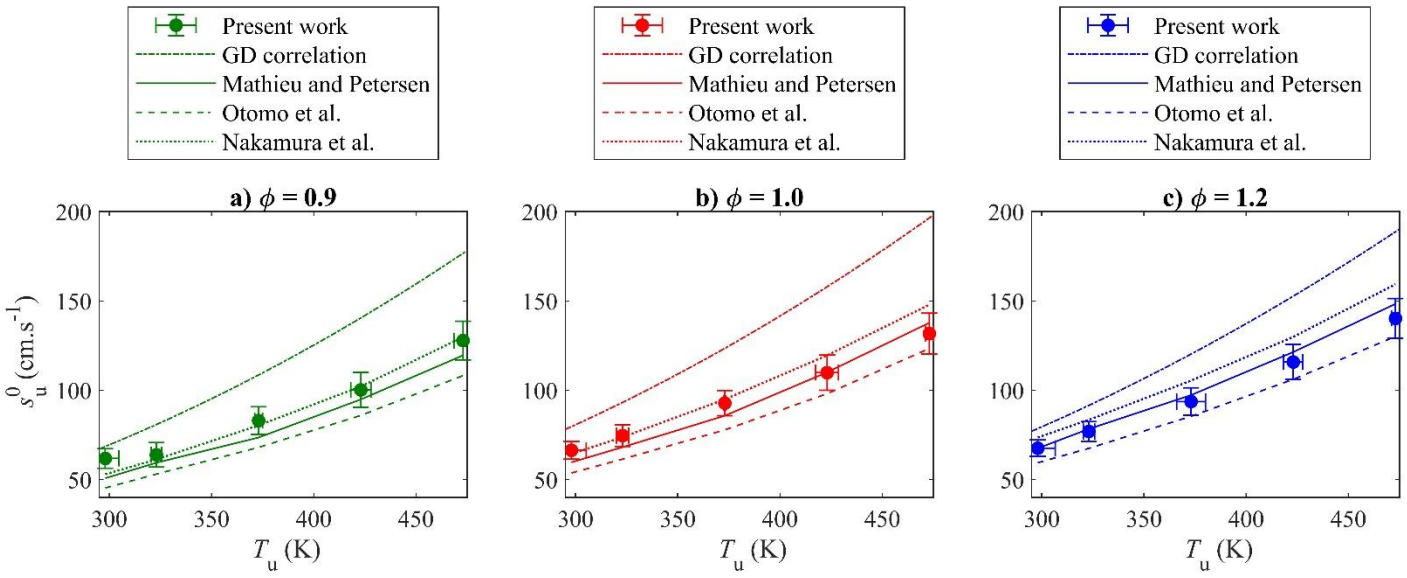

Figure 9. Comparison of the predictive capabilities of various models with respect to the temperature effect on the LBV for P_u = 0.1 MPa and x_{H_2} = 0.6.

3.4. Correlation optimization

In an attempt to optimize the correlations proposed by Goldmann and Dinkelacker [32], the new experimental dataset was used to adjust the coefficient correlations for $P_u \leq 0.5$ MPa and $T_u \leq 700$ K. To that end, the present LBV experimental dataset was consolidated with the literature data [10,11,20–22,12–19] and used to fit the correction factor κ by means of a least-squares algorithm. The form of the correction factor was extended by introducing two new coefficients k_5 and k_6 to take into account the temperature dependence, analogously to the pressure dependence: $\kappa = k_1 k_2^{p_n} p_n^{k_3} (1/\phi)^{k_4} k_5^{T_n} T_n^{k_6}$. In each case, the accuracy of the obtained correlation is assessed by the mean absolute percentage error $M_\emptyset$, the maximum absolute percentage error M_{max}, the minimum absolute percentage error M_{min} and the coefficient of determination R^2 over the considered dataset of size *N*, as in [32]. Different comparisons were conducted and are summarized for the NH_3/air and NH_3/H_2/air correlations in Table 2 and Table 3, respectively.

Unsurprisingly, the GD correlation compares well with the consolidated experimental dataset for NH_3/air mixtures as seen in Table 2, since a satisfactory agreement was found with the new experimental data at elevated temperatures in Sec. 3.1 and 3.3. The extended correlation with the new coefficients of

Table 4 presents a slightly worsened mean absolute percentage error but a better coefficient of determination than the GD correlation.

Table 2. Accuracy of the NH_3/air correlation against experiments for $P_u \leq 0.5$ MPa.

Comparison	T_u	M_{min} (%)	$M_{\emptyset}$ (%)	M_{max} (%)	R^2	N
GD vs. previous literature data	≤ 300 K	0.28	15.0	47.06	0.795	82
GD vs. consolidated data	≤ 473 K	0.08	12.04	47.06	0.948	122
New coefficients vs. consolidated data	≤ 473 K	0.13	13.05	58.41	0.9664	122

However, Table 3 shows that the new consolidated dataset does not compare well with the GD correlation for NH_3/H_2/air mixtures, since $M_{\emptyset}$ increases from 8.26 % to 11.56 % and R^2 drops from 0.977 to 0.867. This was expected following the discrepancies observed in Sec. 3.1, 3.2 and 3.3 between the GD correlation and the present experimental values, especially at high hydrogen fractions. For this reason, a comparison between the GD correlation and the experimental dataset for $0 < x_{H_2} \leq 0.4$ was attempted. The original correlation proved to be slightly more accurate in that case, though not reaching the accuracy shown against the former experimental dataset. Thus, the present attempts to fit the new correlation on the new consolidated dataset resulted in a poorer accuracy when considering the entire H_2 range. Considering that the original correlation behaves differently for small and large hydrogen fractions, it was decided to apply the optimization only in the range $0 < x_{H_2} \leq 0.4$, leading to an improvement in accuracy of the correlation against the consolidated dataset, as seen in Table 3.

Table 3. Accuracy of the NH_3/H_2/air correlation against experiments for $P_u \leq 0.5$ MPa.

Comparison	x_{H_2}	T_u	M_{min} (%)	$M_{\emptyset}$ (%)	M_{max} (%)	R^2	N
GD vs. previous literature data	]0 – 0.6]	≤ 300 K	0.05	8.26	36.55	0.977	93
GD vs. consolidated data	]0 – 0.6]	≤ 473 K	0.03	11.56	49.15	0.867	418
GD vs. consolidated data	]0 – 0.4]	≤ 473 K	0.03	10.31	41.72	0.963	295

[Tapez ici]

New coefficients vs. consolidated data	]0 – 0.4]	≤ 473 K	0.02	9.15	47.24	0.971	295

The corresponding coefficients in Table 4 can be used for the correction factor κ in LBV calculations in the range $0 \leq x_{H_2} \leq 0.4$, all other coefficients in the GD correlations remaining unchanged compared to [32]. However, the new correlation estimates the consolidated dataset less accurately than the original GD correlation estimates the original dataset. Ultimately, a better understanding of the role of NH_3 and H_2 reactions in the detailed kinetic mechanisms should help in better predicting the laminar burning velocity, especially for mixtures containing very low or very high hydrogen fractions. Refined mechanisms could then be used to establish more reliable correlations for reduced computational intensity.

Table 4. New coefficients for the empirical correction factor κ with temperature dependence.

Case	k_1	k_2	k_3	k_4	k_5	k_6
NH_3/air	1.9112	1.0019	-0.0444	0.3526	0.7444	-0.1078
NH_3/H_2/air x_{H_2} =]0 – 0.4]	2.0873	1.0081	-0.1559	0.5383	0.7357	-0.0702

4. Summary and conclusions

An extensive new experimental dataset of ammonia/air and ammonia/hydrogen/air laminar burning velocities was obtained at atmospheric pressure for equivalence ratios ranging from 0.8 to 1.4, hydrogen fractions in the fuel from 0 % to 60 % and unburned gas temperatures from 298 to 473 K by means of the outwardly propagating spherical flame method. Experimental hardware, imaging, radiation-induced and statistical errors were taken into account. Results are in good agreement with previous measurements from the literature obtained with the same method and the heat flux method under NTP, but discrepancies are observed with measurements obtained with the Bunsen burner method for high hydrogen fractions. More than 260 new data points are presented, that significantly enrich the literature data, especially at high temperatures and hydrogen fuel fractions.

A comparison of the present measurements with the LBV correlations recently developed by Goldmann and Dinkelacker, as well as with chemical kinetic simulations using state-of-the-art reaction mechanisms, led to the following summary:

1. The original NH_3/air correlation agrees well with the present experimental data for all temperatures, thus validating its ability to accurately approximate the LBV of mixtures at higher temperatures.
2. The original NH_3/H_2/air correlation underestimates the LBV of rich mixtures with low hydrogen fractions, while it generally overestimates the LBV of mixtures with high hydrogen fractions, especially at elevated temperature and regardless of the equivalence ratio. The LBV of mixtures with intermediate hydrogen fractions are estimated satisfactorily in most cases. This is explained by the better accuracy and availability of experimental data in that range at the time the correlation was first developed.
3. The influence of the temperature is reproduced satisfactorily by the NH_3/H_2/air correlation, except for mixtures with $x_{H_2} \geq 0.5$, where the influence of the temperature is again overestimated.
4. Current reaction mechanisms show satisfactory agreement with the present experimental data over the whole range of investigation, but a significant scatter remains between them.
5. An attempt to optimize the correlations by fitting them on the new consolidated experimental dataset through an experimental correction factor was successful for a limited set of conditions only.

As a result, while the detailed kinetic mechanisms may still require some fine tuning to improve their accuracy, the development of new LBV correlations for NH_3/H_2 fuels requires careful validation based on fully validated reaction mechanisms and accurate experimental data. However, the present optimization proposed for the GD correlations should allow to conduct turbulent combustion simulations with satisfactory accuracy and low computational cost for hydrogen fractions in the fuel smaller than 50%.

Acknowledgements

[Tapez ici]

The research leading to these results has received funding from the French Government's "Investissement d'Avenir" program: "Laboratoire d'Excellence CAPRYSSES" (Grant No ANR-11- LABX-0006-01).

References

[1] UNFCCC. Paris Agreement. Paris: 2015.

[2] Rogelj J, Shindell D, Jiang K, Fifita S, Forster P, Ginzburg V, et al. Mitigation pathways compatible with 1.5°C in the context of sustainable development. IPCC Spec Rep 2018:93–174.

[3] Tatin A, Bonin J, Robert M. A Case for Electrofuels. ACS Energy Lett 2016:1062–4. doi:10.1021/acsenergylett.6b00510.

[4] Zamfirescu C, Dincer I. Using ammonia as a sustainable fuel. J Power Sources 2008;185:459–65. doi:10.1016/j.jpowsour.2008.02.097.

[5] Giddey S, Badwal SPS, Munnings C, Dolan M. Ammonia as a Renewable Energy Transportation Media. ACS Sustain Chem Eng 2017;5:10231–9. doi:10.1021/acssuschemeng.7b02219.

[6] Cheema II, Krewer U. Operating envelope of Haber–Bosch process design for power-to-ammonia. RSC Adv 2018;8:34926–36. doi:10.1039/C8RA06821F.

[7] Grinberg Dana A, Elishav O, Bardow A, Shter GE, Grader GS. Nitrogen-Based Fuels: A Power-to-Fuel-to-Power Analysis. Angew Chemie - Int Ed 2016;55:8798–805. doi:10.1002/anie.201510618.

[8] Valera-Medina A, Xiao H, Owen-Jones M, David WIF, Bowen PJ. Ammonia for power. Prog Energy Combust Sci 2018;69:63–102. doi:10.1016/j.pecs.2018.07.001.

[9] Kobayashi H, Hayakawa A, Somarathne KDKA, Okafor EC. Science and technology of ammonia combustion. Proc Combust Inst 2019;37:109–33. doi:10.1016/j.proci.2018.09.029.

[10] Zakaznov VF, Kursheva LA, Fedina ZI. Determination of normal flame velocity and critical diameter of flame extinction in ammonia-air mixture. Combust Explos Shock Waves 1978;14:710–3. doi:10.1007/BF00786097.

[11] Ronney PD. Effect of Chemistry and Transport Properties on Near-Limit Flames at Microgravity. Combust Sci Technol 1988;59:123–41. doi:10.1080/00102208808947092.

[12] Pfahl UJ, Ross MC, Shepherd JE, Pasamehmetoglu KO, Unal C. Flammability limits, ignition energy, and flame speeds in H2-CH4-NH3-N2O-O2-N2 mixtures. Combust Flame 2000;123:140–58.

510 doi:10.1016/S0010-2180(00)00152-8.
511 [13] Jabbour T, Clodic DF. Burning Velocity and Refrigerant Flammability Classification. Trans - Am Soc
512 Heat Refrig Air Cond Eng 2004;110:522–33.
513 [14] Takizawa K, Takahashi A, Tokuhashi K, Kondo S, Sekiya A. Burning velocity measurements of
514 nitrogen-containing compounds. J Hazard Mater 2008;155:144–52.
515 doi:10.1016/j.jhazmat.2007.11.089.
516 [15] Hayakawa A, Goto T, Mimoto R, Arakawa Y, Kudo T, Kobayashi H. Laminar burning velocity and
517 Markstein length of ammonia/air premixed flames at various pressures. Fuel 2015;159:98–106.
518 doi:10.1016/j.fuel.2015.06.070.
519 [16] Davis SG, Pagliaro JL, Debold TF, van Wingerden M, van Wingerden K. Flammability and explosion
520 characteristics of mildly flammable refrigerants. J Loss Prev Process Ind 2017;49:662–74.
521 doi:10.1016/j.jlp.2017.05.019.
522 [17] Mei B, Zhang X, Ma S, Cui M, Guo H, Cao Z, et al. Experimental and kinetic modeling investigation
523 on the laminar flame propagation of ammonia under oxygen enrichment and elevated pressure
524 conditions. Combust Flame 2019;210:236–46. doi:10.1016/j.combustflame.2019.08.033.
525 [18] Lee JH, Lee SI, Kwon OC. Effects of ammonia substitution on hydrogen/air flame propagation and
526 emissions. Int J Hydrogen Energy 2010;35:11332–41. doi:10.1016/j.ijhydene.2010.07.104.
527 [19] Lee JH, Kim JH, Park JH, Kwon OC. Studies on properties of laminar premixed hydrogen-added
528 ammonia/air flames for hydrogen production. Int J Hydrogen Energy 2010;35:1054–64.
529 doi:10.1016/j.ijhydene.2009.11.071.
530 [20] Li J, Huang H, Kobayashi N, He Z, Nagai Y. Study on using hydrogen and ammonia as fuels:
531 Combustion characteristics and NOx formation. Int J Energy Res 2014;38:1214–23.
532 doi:10.1002/er.3141.
533 [21] Ichikawa A, Hayakawa A, Kitagawa Y, Kunkuma Amila Somarathne KDD, Kudo T, Kobayashi H.
534 Laminar burning velocity and Markstein length of ammonia/hydrogen/air premixed flames at elevated
535 pressures. Int J Hydrogen Energy 2015;40:9570–8. doi:10.1016/j.ijhydene.2015.04.024.
536 [22] Han X, Wang Z, Costa M, Sun Z, He Y, Cen K. Experimental and kinetic modeling study of laminar

burning velocities of NH3/air, NH3/H2/air, NH3/CO/air and NH3/CH4/air premixed flames. Combust Flame 2019;206:214–26. doi:10.1016/j.combustflame.2019.05.003.

[23] Kumar P, Meyer TR. Experimental and modeling study of chemical-kinetics mechanisms for H2-NH3-air mixtures in laminar premixed jet flames. Fuel 2013;108:166–76. doi:10.1016/j.fuel.2012.06.103.

[24] Miller JA, Smooke MD, Green RM, Kee RJ. Kinetic Modeling of the Oxidation of Ammonia in Flames. Combust Sci Technol 1983;34:149–76. doi:10.1080/00102208308923691.

[25] Lindstedt RP, Lockwood FC, Selim MA. Detailed kinetic modelling of chemistry and temperature effects on ammonia oxidation. Combust Sci Technol 1994;99:253–76. doi:10.1080/00102209408935436.

[26] Tian Z, Li Y, Zhang L, Glarborg P, Qi F. An experimental and kinetic modeling study of premixed NH3/CH4/O2/Ar flames at low pressure. Combust Flame 2009;156:1413–26. doi:10.1016/j.combustflame.2009.03.005.

[27] Konnov AA. Implementation of the NCN pathway of prompt-NO formation in the detailed reaction mechanism. Combust Flame 2009;156:2093–105. doi:10.1016/j.combustflame.2009.03.016.

[28] Okafor EC, Naito Y, Colson S, Ichikawa A, Kudo T, Hayakawa A, et al. Experimental and numerical study of the laminar burning velocity of CH4–NH3–air premixed flames. Combust Flame 2018;187:185–98. doi:10.1016/j.combustflame.2017.09.002.

[29] Cavaliere R, Costa M, Bai XS, da Rocha RC, Costa M, Bai XS, et al. Chemical kinetic modelling of ammonia/hydrogen/air ignition, premixed flame propagation and NO emission. Fuel 2019;246:24–33. doi:10.1016/j.fuel.2019.02.102.

[30] Mathieu O, Petersen EL. Experimental and modeling study on the high-temperature oxidation of Ammonia and related NOx chemistry. Combust Flame 2015;162:554–70. doi:10.1016/j.combustflame.2014.08.022.

[31] Otomo J, Koshi M, Mitsumori T, Iwasaki H, Yamada K. Chemical kinetic modeling of ammonia oxidation with improved reaction mechanism for ammonia/air and ammonia/hydrogen/air combustion. Int J Hydrogen Energy 2018;43:3004–14. doi:10.1016/j.ijhydene.2017.12.066.

[Tapez ici]

564 [32] Goldmann A, Dinkelacker F. Approximation of laminar flame characteristics on premixed
565 ammonia/hydrogen/nitrogen/air mixtures at elevated temperatures and pressures. Fuel 2018;224:366–
566 78. doi:10.1016/j.fuel.2018.03.030.
567 [33] Metghalchi M, Keck JC. Burning velocities of mixtures of air with methanol, isooctane, and indolene
568 at high pressure and temperature. Combust Flame 1982;48:191–210. doi:10.1016/0010-
569 2180(82)90127-4.
570 [34] Galmiche B, Halter F, Foucher F. Effects of high pressure, high temperature and dilution on laminar
571 burning velocities and Markstein lengths of iso-octane/air mixtures. Combust Flame 2012;159:3286–
572 99. doi:10.1016/j.combustflame.2012.06.008.
573 [35] Brequigny P, Endouard C, Mounaïm-Rousselle C, Foucher F. An experimental study on turbulent
574 premixed expanding flames using simultaneously Schlieren and tomography techniques. Exp Therm
575 Fluid Sci 2018;95:11–7. doi:10.1016/j.expthermflusci.2017.12.018.
576 [36] Huo J, Yang S, Ren Z, Zhu D, Law CK. Uncertainty reduction in laminar flame speed extrapolation
577 for expanding spherical flames. Combust Flame 2018;189:155–62.
578 doi:10.1016/j.combustflame.2017.10.032.
579 [37] Kelley AP, Law CK. Nonlinear effects in the extraction of laminar flame speeds from expanding
580 spherical flames. Combust Flame 2009;156:1844–51. doi:10.1016/j.combustflame.2009.04.004.
581 [38] Ronney PD, Sivashinsky GI. A Theoretical Study of Propagation and Extinction of Nonsteady
582 Spherical Flame Fronts. SIAM J Appl Math 1989;49:1029–46. doi:https://doi.org/10.1137/0149062.
583 [39] Halter F, Tahtouh T, Mounaïm-Rousselle C. Nonlinear effects of stretch on the flame front
584 propagation. Combust Flame 2010;157:1825–32. doi:10.1016/j.combustflame.2010.05.013.
585 [40] Moffat RJ. Describing the uncertainties in experimental results. Exp Therm Fluid Sci 1988;1:3–17.
586 doi:10.1016/0894-1777(88)90043-X.
587 [41] Brequigny P, Uesaka H, Sliti Z, Segawa D, Foucher F, Dayma G, et al. Uncertainty in measuring
588 laminar burning velocity from expanding methane-air flames at low pressures. 11th Mediterr.
589 Combust. Symp., Tenerife, Spain: 2019.
590 [42] Yu H, Han W, Santner J, Gou X, Sohn CH, Ju Y, et al. Radiation-induced uncertainty in laminar

591 flame speed measured from propagating spherical flames. Combust Flame 2014;161:2815–24.
592 doi:10.1016/j.combustflame.2014.05.012.
593 [43] Nakamura H, Shindo M. Effects of radiation heat loss on laminar premixed ammonia/air flames. Proc
594 Combust Inst 2019;37:1741–8. doi:10.1016/j.proci.2018.06.138.
595 [44] Nakamura H, Hasegawa S, Tezuka T. Kinetic modeling of ammonia/air weak flames in a micro flow
596 reactor with a controlled temperature profile. Combust Flame 2017;185:16–27.
597 doi:10.1016/j.combustflame.2017.06.021.
598 [45] ANSYS Chemkin-Pro 2019.
599